

Kremer-Grest models for commodity polymer melts: Linking theory, experiment and simulation at the Kuhn scale

Carsten Svaneborg,^{1,*} Hossein Ali Karimi-Varzaneh,² Nils Hojdis,² Frank Fleck,² and Ralf Everaers³

¹*University of Southern Denmark, Campusvej 55, DK-5230 Odense M, Denmark*

²*Continental, PO Box 169, D-30001 Hannover, Germany*

³*Univ Lyon, ENS de Lyon, Univ Claude Bernard, CNRS,*

Laboratoire de Physique and Centre Blaise Pascal, F-69342 Lyon, France

The Kremer-Grest (KG) polymer model is a standard model for studying generic polymer properties in Molecular Dynamics simulations. It owes its popularity to its simplicity and computational efficiency, rather than its ability to represent specific polymers species and conditions. Here we show, that by tuning the chain stiffness it is possible to adapt the KG model to model melts of real polymers. In particular, we provide mapping relations from KG to SI units for a wide range of commodity polymers. The connection between the experimental and the KG melts is made at the Kuhn scale, i.e. at the crossover from chemistry-specific small scale to the universal large scale behavior. We expect the KG models to faithfully represent universal properties dominated by the large scale conformational statistics and dynamics of flexible polymers. In particular, we observe very good agreement between entanglement moduli of our KG models and the experimental moduli of the target polymers.

PACS numbers:

I. INTRODUCTION

Polymers are long chain molecules built by covalent linkage of a large numbers of identical monomers [1, 2]. Some properties of polymeric materials such as their density, their ability to form semi-cristalline phases or their glass transition temperature depend on specific chemical details at the monomer scale. Others, like the variation of the melt viscosity with the molecular weight of the chains, are controlled by the large scale conformational statistics and dynamics of long entangled chains adopting interpenetrating random walk conformations [3]. These latter properties, which are characteristic of polymeric systems, are universal [3, 4] in the sense that a large number of chemically different systems have the same properties, when expressed in suitable material-specific units.

The character of the target properties is crucial for making an intelligent choice of which model to apply in a theoretical or computational investigation. Universal properties can be predicted using simple, analytically or numerically convenient lattice and off-lattice models, see e.g. refs. [3, 5–8] for reviews. In contrast, predicting specific material properties for a given chemical species often requires atom-scale modeling [9]. A growing body of work aims at developing such coarse-grained (CG) polymer models [10–14] designed for specific polymer chemistries such as polyethylene [15–17], polyisoprene [18–21], polystyrene [22–24], polyamide [25, 26], polymethacrylate [27], polydimethylsiloxane [21], bisphenol-A polycarbonate [28–30], polybutadiene [31], polyvinyl [32], and polyisobutylene [21].

Common to these approaches is the selected inclusion of specific chemical details in the coarse-grained models. They offer insights into which atomistic details of the chemical structure are relevant for particular non-universal polymer properties. The inclusion of molecular details is supposed to preserve a certain degree of transferability, i.e. models optimized to describe materials at one state point are expected to remain approximately valid at neighboring state points. [13, 33, 34] Similarly, careful coarse-graining is supposed to assure representability, i.e. the ability of a model to predict properties that it was not explicitly designed to reproduce. [35]

In the present paper, we use a minimal route to include specificity into a generic polymer model, where non-trivial large scale properties *emerge* through the same mechanisms as in the experimental target materials. With universality assuring the strongest form of representability, we expect that by matching a very limited number of conformational properties [36], we can 1) design generic polymer models that match universal properties of real chemical polymers, and 2) map simulation results for such models to real units and hence make quantitative predictions for target polymer systems.

These generic polymer models display complex emergent phenomena. For instance, static and dynamic entanglement effects including multichain mechanisms such as constraint release [37–41] and crumpling [42–45] as well as correlation hole effects [46] will naturally emerge in such models, without the description needing to be accurate on the atomic scale. Polydispersity, branching [47], chemical cross-linking [48–50], and network aging [51] are also straightforward to include. Furthermore, such models can be used to study effects of spatial confinement [52] in thin films [53] and brushes [54–56] or the addition of filler particles in composite materials [57, 58], or the weld-

*Electronic address: science@zqex.dk

ing dynamics at polymer interfaces [59, 60] to name a few examples.

Here we apply this philosophy to the most popular off-lattice polymer model introduced by Kremer and Grest (KG) [61, 62]. In the KG model approximately hard sphere beads are connected by strong non-linear springs generating the connectivity and the liquid-like monomer packing characteristic of polymer melts. The spring potential is chosen to energetically prevent two polymer chains from passing through each other and thus to assure that the model reproduces the microscopic topological constraints dominating the dynamics of long-chain polymers [62]. The KG model is formulated in the natural units of the Lennard-Jones potential describing the interaction potential between beads. The energy scale ϵ together with the bead diameter, σ , and mass, m_b , define the standard Lennard-Jones system of units including the time scale $\tau = \sigma\sqrt{m_b/\epsilon}$.

The purpose of this paper is to establish KG simulations as a convenient tool for exploring emergent universal properties of *specific* polymer materials. To obtain valid coarse-grain descriptions for commodity polymer melts, we tune the strength of a bending potential introduced into the model by Faller and Müller-Plathe [63–65]. The proposed mapping relies on results of a preceding paper, where we have studied the dependence of the characteristic time and length scales in KG bead-spring polymer melts on this parameter [66]. Here we provide tables specifying a one-parameter KG force field for a wide range of experimental polymer melts, i.e. we 1) list which bending stiffness to use for modelling a particular chemical polymer species, and 2) how to translate simulation results expressed in KG units into predictions for the specific polymer material expressed in SI units. Note that while we provide force-fields for materials like polyethylene (PE), polyoxymethylene (POM), polyethylene terephthalate (PET), polybutylene terephthalate (PBT), polytetrafluoroethylene (PTFE) or isotactic polypropylene (i-PP), they cannot be expected to reproduce the tendency to form semi-crystalline ordering. Such KG models should thus be taken with a grain of salt or, maybe, as a reminder that there is more to polymers than universal properties. Nonetheless, we note that coarse-grain models have been used to study crystallization [67], and recently specialized KG models were developed and optimized [68, 69] to study crystallization phenomena.

The paper is structured as follows; We introduce the Kuhn scale in Sec. II. After characterizing experimental (IIB) and KG (IIC) melts in the corresponding units, we derive mapping relations for static (IID) and dynamic (IIE) properties. Sec. III reviews theoretical insights into the emergence of universal polymer behavior beyond the Kuhn scale in an attempts to outline the types of problems to which Kuhn matched KG models may be profitably applied. As a practical application, we compare plateau moduli inferred from KG models to experimental values. The discussion in Sec. IV focuses on the

place of Kuhn scale matched KG models within the multiscale hierarchy of polymer polymers. We propose to view Kuhn scale matching as a special case of structure based coarse-graining, explain the advantages of matching the KG model to experiments on the Kuhn rather than the entanglement scale, and discuss the large effective time step of our models together with the expected speedup relative to atomistic simulations. Finally, we briefly conclude in Sec. V.

II. MATCHING AT THE KUHN SCALE

The natural units of polymer physics [3, 4, 70] are the mesoscopic Kuhn units: the Kuhn length, l_K , the Kuhn time, τ_K , and $k_B T$ as the natural energy scale in entropy dominated systems. Kuhn’s seminal insight in the 1930s was to use an N_K step random walk of segment length l_K to describe the large scale chain conformations [71]. For the proper choice of l_K , the Kuhn model reproduces both, the end-to-end distance at full extension, $L = l_K N_K$, and the mean-square end-to-end distance, $\langle R^2 \rangle = N_K l_K^2$, of the target polymer. In particular, flexible polymers exhibit *universal* behavior [3, 4, 70] beyond the Kuhn scale defined by l_K and the corresponding time scale τ_K . In contrast, behavior on smaller scales is material specific and dependent on atomic details. For example, the large scale flexibility has completely different microscopic origins in the wormlike chain [72] and in the rotational-isomeric-state [2] models. Similarly, there are well-documented exceptions [73] to the strong form of time-temperature superposition principle, which postulates identical temperature dependence for *all* microscopic relaxation mechanisms down to the atomic scale. When it comes to linking theory, experiments, atomistic and coarse-grain simulation, then we believe that the natural approach is to match them at the Kuhn scale.

A. The Kuhn scale

The Kuhn length,

$$l_K = \frac{\langle R^2 \rangle}{L}, \quad (1)$$

characterizes the crossover from local rigid rod to random walk behavior.

It is not straightforward to infer the Kuhn length from the chemical structure of a polymer in its melt state as it depends on intramolecular interactions, chemistry-specific local packing, and universal long-range correlations [2, 46]. However, a known Kuhn length can be used to characterize the large scale structure of polymer melts via two related dimensionless numbers.

The first such number is a dimensionless measure of chain length, the number of Kuhn segments per chain:

$$N_K = \frac{\langle R^2 \rangle}{l_K^2} = \frac{L^2}{\langle R^2 \rangle}, \quad (2)$$

The second number, to which we refer as the Kuhn number, is a dimensionless measure of density,

$$n_K = \overline{\rho}_K l_K^3, \quad (3)$$

defined as the number of Kuhn segments within the volume of a Kuhn length cube.

To characterise the dynamics, one can define the friction coefficient, ζ_K , of a Kuhn segment undergoing Brownian motion. Interpreting ζ_K as a viscous Stokes drag, $\zeta_K \propto \eta_K l_K$, it is convenient to define an effective viscosity at the Kuhn scale as

$$\eta_K = \frac{1}{36} \frac{\zeta_K}{l_K}. \quad (4)$$

The fundamental time scale of the dynamics of intrinsically flexible polymers is set by the time that it takes a Kuhn segment to diffuse ($D_K = k_B T / \zeta_K$) over a distance comparable to its own size. Again it turns out to be practical to incorporate some numerical prefactors into the definition of the Kuhn time:

$$\tau_K = \frac{1}{3\pi^2} \frac{\zeta_K l_K^2}{k_B T} = \frac{12}{\pi^2} \frac{\eta_K l_K^3}{k_B T}. \quad (5)$$

B. Commodity polymer melts at the Kuhn scale

At a given state point (temperature), a melt of monodisperse chains (with molecular weight M_c) can be characterized by just a few experimental observables: the mass density ρ_{bulk} , the average chain end-to-end distance per unit mass $\langle R^2 \rangle / M_c$, and the maximal chain extension, L . Values for these observables for a large number of typical polymers are collected in Ref. [74]. We present data for a selected subset of polymers expressed in Kuhn units in Tab. I. The Kuhn lengths are in the 1–2 nanometer range, with a Kuhn segment mass $M_K = M_c / N_K \sim 100 - 2000$ g/mol. The number of monomers in a Kuhn segment varies in the range of 1–13, and the number density of Kuhn segments, ρ_K , varies in the range of $0.5 - 5nm^{-3}$.

A key characteristic of polymer species is their Kuhn number, which varies for common, flexible commodity polymers in the range $2 \leq n_K \leq 12$. For comparison, $n_K \gg 10$ in gels of tightly entangled filamentous proteins such as f-actin.[75] In Tab. I, we observe a strong and systematic correlation between the Kuhn number and emergent properties such as the entanglement modulus and the entanglement length measured in Kuhn units. This observation suggests that the Kuhn number is a key molecular parameter in predicting entanglement related phenomena. We will return to this point in Sec. III.

C. Kremer-Grest model polymer melts at the Kuhn scale

The Kremer-Grest model[61, 62] is a defacto standard model in Molecular Dynamics investigations of generic

polymer properties. The KG model is a bead-spring model, where the mutual interactions between all beads are given by the Weeks-Chandler-Anderson (WCA) potential (the truncated and shifted repulsive part of the 12-6 Lennard-Jones potential),

$$U_{WCA}(r) = 4\epsilon \left[\left(\frac{\sigma}{r} \right)^{-12} - \left(\frac{\sigma}{r} \right)^{-6} + \frac{1}{4} \right] \quad \text{for } r < 2^{1/6}\sigma, \quad (6)$$

where ϵ defines the energy scale and σ the bead diameter. The standard choice for the temperature is $k_B T = \epsilon$. Bonded beads interact through the finite-extensible-nonlinear spring (FENE) potential given by

$$U_{FENE}(r) = -\frac{kR^2}{2} \ln \left[1 - \left(\frac{r}{R} \right)^2 \right]. \quad (7)$$

Choosing a spring constant $k = 30\epsilon\sigma^{-2}$ and a bond length, $R = 1.5\sigma$, where the FENE potential diverges, the bond length is $l_b = 0.965\sigma$. The standard choice for the bead density is $\rho_b = 0.85\sigma^{-3}$. Faller and Müller-Plathe [63–65] augmented the standard KG model with a bending potential,

$$U_{bend}(\Theta) = \kappa (1 - \cos \Theta), \quad (8)$$

where Θ denotes the angle between subsequent bonds.

To prepare the present study, we have investigated the dependence of the characteristic time and length scales in KG bead-spring polymer melts on the reduced bending energy, $x \equiv \beta\kappa = \kappa/k_B T$ [66]. In particular, we found for the Kuhn length:

$$\begin{aligned} l_K(x) &= l_K^{(0)} + \Delta l_K \quad (9) \\ l_K^{(0)}(x)/\sigma &= \frac{l_b}{\sigma} \begin{cases} \frac{2x+e^{-2x}-1}{1-e^{-2x}(2x+1)} & \text{if } x \neq 0 \\ 1 & \text{if } x = 0 \end{cases} \\ \Delta l_K(x)/\sigma &= 0.769888 + 0.776514x \\ &\quad \tanh(0.147244 - 0.405299x - 0.0298337x^2) \end{aligned}$$

From this relation, we can directly infer the dimensionless Kuhn number, Eq. (3), characterising KG melts:

$$n_K(\beta\kappa) = \rho_b \frac{l_b}{l_K} l_K^3. \quad (10)$$

Finally, the number of Kuhn segments between entanglements, the Kuhn friction and Kuhn time of the KG model are given by

$$\begin{aligned} N_{eK}(x) &= 39.130 - 30.237x + 4.2834x^2 \\ &\quad + 3.2065x^3 - 1.2879x^4 + 0.1372x^5 \end{aligned} \quad (11)$$

$$\zeta_K(x)/(m_b/\tau) = 36.021 + 10.149x + 5.6341x^2 \quad (12)$$

$$\begin{aligned} \tau_K(x)/\tau &= 4.2076 + 2.8451x + 1.6485x^2 \\ &\quad + 0.6464x^3 + 0.6524x^4 \end{aligned} \quad (13)$$

The parameterization of the Kuhn length we believe to be valid for arbitrary values for stiffness $\beta\kappa$, while the

name	T_{ref} [K]	$\langle R^2 \rangle / M_c$ [$\text{\AA}^2 \text{mol/g}$]	ρ_{bulk} [g/cm^3]	G_e [MPa]	p [\AA]	d_T [\AA]	n_K	l_K [\AA]	M_K [g/mol]	M_K/M_m	ρ_K [nm^{-3}]	$G_e l_K^3 / k_B T$	N_{eK}	α
PI-50	298	0.528	0.893	0.51	3.52	47.7	2.50	8.80	146.60	2.15	3.66	0.085	29.41	13.6
PI-7	298	0.596	0.900	0.44	3.10	55.1	2.72	8.44	119.60	1.76	4.52	0.064	42.55	17.8
PDMS*	298	0.422	0.970	0.25	4.06	63.7	2.82	11.42	309.28	4.17	1.89	0.091	31.08	15.7
PI-20	298	0.591	0.898	0.44	3.13	54.8	2.86	8.98	136.50	2.00	3.95	0.077	37.17	17.5
PI-34	298	0.585	0.965	0.44	2.94	56.5	3.02	9.58	156.90	2.30	3.44	0.093	32.32	19.2
cis-PBd	298	0.758	0.900	0.95	2.43	42.2	3.40	8.28	90.50	1.67	5.99	0.131	25.93	17.3
PIB(413)	413	0.557	0.849	0.38	3.51	65.8	3.47	12.20	267.90	4.77	1.91	0.119	29.02	18.7
cis-PI	298	0.679	0.910	0.72	2.69	46.0	3.47	9.34	128.60	1.89	4.26	0.144	24.15	17.1
a-PP(463)	463	0.678	0.765	0.53	3.20	61.7	3.53	11.20	183.40	4.36	2.51	0.115	30.59	19.3
i-PP	463	0.694	0.766	0.54	3.12	61.7	3.64	11.40	187.80	4.46	2.46	0.125	29.22	19.8
a-PP(413)	413	0.678	0.791	0.59	3.10	56.0	3.65	11.20	183.40	4.36	2.60	0.145	25.21	18.1
a-PP(348)	348	0.678	0.825	0.60	2.97	51.9	3.81	11.20	183.40	4.36	2.71	0.175	21.70	17.5
a-PP	298	0.678	0.852	0.60	2.87	48.8	3.92	11.20	183.40	4.36	2.79	0.205	19.15	17.0
PIB	298	0.570	0.918	0.43	3.17	55.2	3.94	12.50	274.20	4.89	2.02	0.202	19.52	17.4
a-PMMA	413	0.390	1.130	0.39	3.77	62.5	4.07	15.30	598.00	5.97	1.14	0.243	16.72	16.6
i-PS*	413	0.420	0.969	0.24	4.08	76.7	4.19	17.11	697.12	6.69	0.84	0.209	20.10	18.8
a-PMA	298	0.436	1.110	0.31	3.43	61.9	4.29	14.70	494.60	5.75	1.35	0.241	17.79	18.1
PI-75	298	0.563	0.890	0.46	3.31	51.8	4.53	15.00	399.30	5.86	1.34	0.379	11.94	15.6
PBd-20	298	0.841	0.895	1.34	2.21	37.3	4.54	10.10	122.40	2.26	4.41	0.335	13.55	16.9
a-PS*	413	0.437	0.969	0.25	3.92	76.3	4.54	17.80	725.34	6.96	0.80	0.247	18.35	19.4
PBd-98	300	0.661	0.890	0.71	2.82	45.4	4.83	13.70	284.80	5.27	1.88	0.442	10.93	16.1
PEO*	353	0.805	1.060	2.25	1.95	33.4	4.99	9.71	117.12	2.66	5.45	0.423	11.81	17.1
POM*	473	0.763	1.140	2.12	1.91	40.1	5.06	9.65	122.11	4.07	5.62	0.293	17.28	21.0
a-PHMA	373	0.366	0.960	0.11	4.73	98.4	5.19	24.40	1622.00	9.53	0.36	0.317	16.35	20.8
a-PVA*	333	0.490	1.080	0.44	3.14	57.9	5.26	16.50	555.70	6.45	1.17	0.428	12.30	18.4
SBR	298	0.818	0.913	0.98	2.22	43.6	5.33	11.90	173.60	2.61	3.16	0.399	13.35	19.6
P6N*	543	0.853	0.985	2.25	1.98	41.1	5.53	10.93	140.05	1.24	4.24	0.392	14.11	20.8
a-P α MS*	473	0.442	1.040	0.40	3.61	67.2	5.66	20.43	944.61	7.99	0.66	0.523	10.82	18.6
a-PEA	298	0.463	1.130	0.45	3.17	53.7	5.70	18.10	710.10	7.09	0.96	0.649	8.79	16.9
PET*	548	0.845	0.989	3.88	1.99	31.3	7.50	14.91	263.15	1.37	2.26	1.698	4.42	15.8
s-PP	463	1.030	0.766	1.69	2.10	42.4	7.99	16.90	278.70	6.62	1.66	1.274	6.27	20.2
PE(413)	413	1.250	0.785	3.25	1.69	32.2	8.09	13.70	150.40	5.36	3.14	1.466	5.52	19.0
a-POA	298	0.442	0.980	0.20	3.83	73.3	8.34	31.90	2295.00	12.45	0.26	1.578	5.29	19.1
PC*	473	0.864	1.140	3.38	1.69	33.9	10.93	18.43	393.25	1.55	1.75	3.237	3.38	20.1
PE	298	1.400	0.851	4.38	1.39	26.0	11.10	15.40	168.30	6.00	3.04	3.884	2.86	18.6
PTFE*	653	0.598	1.460	2.12	1.90	47.2	12.30	23.40	915.41	9.15	0.96	3.019	4.07	24.8

TABLE I: Kuhn descriptions and entanglement properties of polymers[74] characterized by experimental temperature T_{ref} , mean-square extension per molecular mass $\langle R^2 \rangle / M_c$, bulk mass density ρ_{bulk} , entanglement modulus G_e , and derived quantities such as the packing length p and tube diameter d_T . The polymers are also characterized by their Kuhn number n_K , Kuhn length l_K , mass of a Kuhn segment M_K , Kuhn density ρ_K , and the reduced entanglement modulus $G_e l_K^3 / [k_B T_{ref}]$, Kuhn segments between entanglements N_{eK} , and number of entanglement strands per entanglement volume α . * denotes polymers where we have derived the Kuhn scale descriptions, for the rest we use the values from Ref. [74]. To uniquely identify polymers, we have added the reference temperature to some of the polymer names.

other relations hold for bending rigidities in the interval $-1 < \beta_\kappa < 2.5$. A negative chain stiffness partly counteracts the stiffness induced by excluded volume interactions between next-nearest beads along a chain, and hence makes the chain more flexible than the standard

KG model.

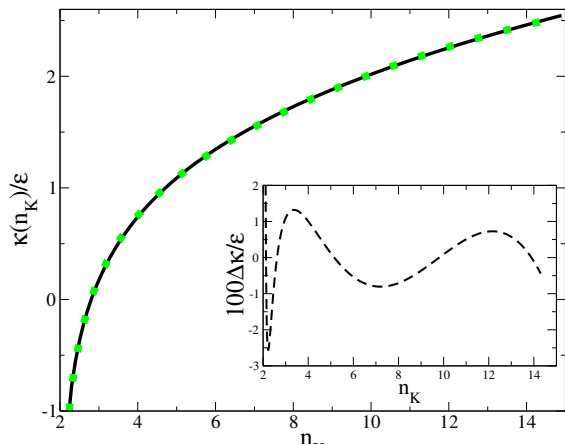


FIG. 1: KG chain stiffness vs. Kuhn number using eq. (10) (solid black line) and our approximate inversion eq. (15) (green symbols). The inset shows the error of our numerical inversion.

D. A one parameter Kremer-Grest “force field” for commodity polymer melts

As a first step in defining a KG force field for a polymeric material we fix the energy scale to the thermal excitation energy [8],

$$\epsilon = k_B T, \quad (14)$$

at the temperature of interest. The key step is the choice of the bending stiffness: we match the dimensionless Kuhn numbers n_K characterising the experimental system and the model polymer melt. A priori, this requires the numerical inversion of the combination of Eqs. (9) and (10). As shown in Fig. 1, the approximate relation

$$\frac{\kappa(n_K)}{k_B T} = 0.822264 \log(n_K - 2.0) - 0.000290834 n_K^3 + 0.00871154 n_K^2 - 0.0552417 n_K + 0.280663 \quad (15)$$

provides an excellent approximation over the experimentally relevant range, $2 \leq n_K \leq 15$. Through eq. (15), l_K , N_{eK} , ζ_K , and τ_K become functions of the Kuhn number. Note that the standard KG model with $\beta\kappa = 0$ essentially corresponds to the intrinsically most flexible polymers such as PDMS or PI with 7–50% 3,4 content.

We can obtain the number of beads per Kuhn length as

$$c_b(n_K) \equiv \frac{l_K}{l_b} = \sqrt{\frac{n_K}{\rho_b l_b^3}} \quad (16)$$

and hence the number of beads required to represent a chain of a given length (molecular mass)

$$N_b = c_b(n_K) N_K. \quad (17)$$

What remains is to fix the mapping relations for the simulation units of length, mass, and time. Equating the

model and experimental Kuhn lengths and accounting for the small difference, $l_b = 0.965\sigma$, between the bond length and the bead diameter in the KG model, we obtain

$$\sigma = \frac{l_K^{exp}}{0.965 \times c_b(n_K)} \quad (18)$$

The bead mass is obtained along the same lines by equating the experimental mass of a Kuhn segment to the mass of a Kuhn segment in the model:

$$m_b = \frac{M_K^{exp}}{c_b(n_K)}. \quad (19)$$

In Table II we have listed the resulting Kremer-Grest model parameters and mappings for the polymer species shown in Tab. I. By construction, the number of beads per Kuhn length is an increasing function of n_K and varies between 1.7 and 3.9. With $-0.4\epsilon \leq \kappa \leq 2.3\epsilon$ the required stiffness parameters falls into the validity range of our empirical relations for Kuhn length, entanglement length, and Kuhn friction. Bead diameters vary between 4 and 10\AA , the energy scale is given by the experimental temperature range and varies within a factor of two. Nevertheless, the KG unit of stress, $4\text{MPa} < \epsilon\sigma^{-3} < 112\text{MPa}$, exhibits a much larger spread. As a rule of thumb, beads correspond to monomers. But there are important variations. To cite some examples,

PI and PDMS (polyisoprene and polydimethylsiloxane) are effectively the most flexible chains, which map fairly well on the standard KG model with $\beta\kappa \equiv 0$. PI beads have a diameter of 5\AA and represent one monomer; PDMS beads have a diameter of 6\AA and represent two monomers.

PS (polystyrene) beads represent three monomers and have with 7.6\AA a correspondingly larger diameter.

PE (polyethylene) is among the effectively stiffest chains, which 4 beads per Kuhn length and $\beta\kappa \approx 2$. PE beads represent 1.5 monomers; with 4\AA they are relatively small.

PC (polycarbonate) is comparable to PE in effective stiffness. With a diameter of 5\AA , PC beads are comparable to PI beads. However, in the case of PC 2.5 beads are required to represent the more complex monomers, which is remarkably similar to 2 bead / ellipsoid models per monomer used by Tschoeb et al.[28]

A priori, the parameters listed in Table II are only valid at the indicated reference temperatures, where the chain dimensions were determined experimentally. To model polymer melts at different temperatures, we have, in principle, to account for changes in (i) the single chain statistics and (ii) the overall density. It is straightforward to translate a temperature dependent Kuhn length, $l_K = l_K(T)$, into a temperature dependent bending *free*

name	n_K	$\beta\kappa$	c_b	l_K/σ	M_m/M_b	$M_b/[g/mol]$	$\epsilon/10^{-21}J$	σ/nm	$\epsilon\sigma^{-3}/MPa$
PI-50	2.50	-0.378	1.81	1.74	0.84	81.13	4.11	0.50	32.0
PI-7	2.72	-0.086	1.89	1.82	1.07	63.37	4.11	0.46	41.3
PDMS*	2.82	0.013	1.92	1.85	0.46	161.05	4.11	0.62	17.6
PI-20	2.86	0.056	1.94	1.87	0.97	70.50	4.11	0.48	37.1
PI-34	3.02	0.191	1.99	1.92	0.86	78.86	4.11	0.50	33.1
cis-PBd	3.40	0.445	2.11	2.04	1.26	42.87	4.11	0.41	61.3
PIB(413)	3.47	0.483	2.13	2.06	0.45	125.69	5.70	0.59	27.3
cis-PI	3.47	0.484	2.13	2.06	1.13	60.32	4.11	0.45	44.0
a-PP(463)	3.53	0.518	2.15	2.07	0.49	85.25	6.39	0.54	40.7
i-PP	3.64	0.575	2.18	2.11	0.49	85.96	6.39	0.54	40.4
a-PP(413)	3.65	0.580	2.19	2.11	0.50	83.84	5.70	0.53	38.2
a-PP(348)	3.81	0.656	2.23	2.16	0.51	82.08	4.80	0.52	34.3
a-PP	3.92	0.708	2.27	2.19	0.52	80.84	4.11	0.51	30.7
PIB	3.94	0.714	2.27	2.19	0.47	120.66	4.11	0.57	22.2
a-PMMA	4.07	0.770	2.31	2.23	0.39	258.82	5.70	0.69	17.6
i-PS*	4.19	0.819	2.35	2.26	0.35	297.22	5.70	0.76	13.2
a-PMA	4.29	0.856	2.37	2.29	0.41	208.42	4.11	0.64	15.6
PI-75	4.53	0.941	2.44	2.35	0.42	163.78	4.11	0.64	15.9
PBd-20	4.54	0.944	2.44	2.35	1.08	50.16	4.11	0.43	52.2
a-PS*	4.54	0.944	2.44	2.35	0.35	297.19	5.70	0.76	13.2
PBd-98	4.83	1.039	2.52	2.43	0.48	113.08	4.14	0.56	23.1
PEO*	4.99	1.086	2.56	2.47	0.96	45.77	4.87	0.39	80.2
POM*	5.06	1.105	2.58	2.48	0.63	47.40	6.53	0.39	111.5
a-PHMA	5.19	1.143	2.61	2.52	0.27	621.59	5.15	0.97	5.7
a-PVA*	5.26	1.162	2.63	2.53	0.41	211.52	4.60	0.65	16.7
SBR	5.33	1.182	2.65	2.55	1.01	65.62	4.11	0.47	40.6
P6N*	5.53	1.234	2.69	2.60	2.18	51.98	7.50	0.42	100.9
a-P α MS*	5.66	1.265	2.72	2.63	0.34	346.66	6.53	0.78	13.9
a-PEA	5.70	1.276	2.74	2.64	0.39	259.56	4.11	0.69	12.8
PET*	7.50	1.646	3.14	3.03	2.29	83.82	7.57	0.49	63.4
s-PP	7.99	1.728	3.24	3.12	0.49	86.03	6.39	0.54	40.5
PE(413)	8.09	1.744	3.26	3.14	0.61	46.15	5.70	0.44	69.0
a-POA	8.34	1.785	3.31	3.19	0.27	693.22	4.11	1.00	4.1
PC*	10.93	2.136	3.79	3.65	2.45	103.76	6.53	0.50	51.0
PE	11.10	2.156	3.82	3.68	0.64	44.07	4.11	0.42	56.4
PTFE*	12.30	2.291	4.02	3.87	0.44	227.70	9.02	0.60	41.1

TABLE II: Kremer-Grest model parameters for the polymers shown in Tab. I in terms of the Kuhn number, bending stiffness $\beta\kappa$, number of beads per Kuhn segment c_b , Kuhn length expressed in KG units, number of beads per monomer M_m/m_b , and finally the conversion relations from KG units for energy ϵ , length σ , and stress $\epsilon\sigma^{-3}$ to SI units.

energy, $\kappa = \kappa(T)$, of our coarse-grain model. To a first approximation, $\kappa(T)$ can be written in the form $\kappa(T) = \kappa_h - \kappa_s T$, where κ_h and κ_s are the enthalpic and entropic contributions to the stiffness.[76] Since the Kuhn length of the KG model, Eq. (9), depends on the *reduced* bending free energy, $x = \kappa(T)/k_B T$, a temperature-independent Kuhn length corresponds to a bending free energy of *entropic* origin. Note, however, that density changes and the corresponding temperature variations in n_K result in less intuitive shifts in bead diameters and

weights with temperature. This is a consequence of our choice to preserve the ‘‘canonical’’ KG bead density of $\rho_b = 0.85\sigma^{-3}$.

In practice, the static melt properties are relatively insensitive to changes of temperature: the relative density expansion coefficient is $d \ln \rho_{bulk}/dT \approx -6 \times 10^{-4} K^{-1}$, while typical thermal chain expansion coefficients $|d \ln \langle R^2 \rangle(T)/dT| < 10^{-3} K^{-1}$. [74] Since $n_K(T) \sim \rho_{bulk} \langle R^2 \rangle^2$, we obtain $|d \ln n_K(T)/dT| < 3 \times 10^{-3} K^{-1}$. In the one case where Ref. [74] provides data, atactic

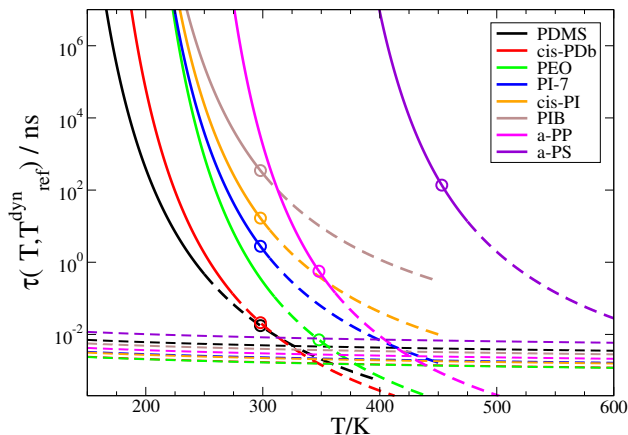


FIG. 2: KG time unit τ in ns as function of temperature for a number of polymer species listed in the legend and distinguished by color. Typical time steps in simulations are $\delta t = 10^{-2}\tau$. Solid lines: WLF-extrapolation over the temperature range $[T_g, T_g + 100K]$, Thick dashed lines: WLF-extrapolation for $T > T_g + 100K$, Symbols: Estimate of τ derived from experimental data for the dynamic reference temperature, T_{ref}^{dyn} , underlying the WLF extrapolation. Thin dashed lines: standard estimation of the LJ time $\tau = \sigma\sqrt{M_b}/\epsilon$ using the mapping values for bead diameter, mass, and energy scale.

polypropylene, the 50% increase in temperature over the interval $298K \leq T \leq 463K$ causes a slight increase in density while apparently leaving the chain dimensions unchanged. The corresponding reduction of the Kuhn number from $n_K = 3.92$ to $n_K = 3.43$, suggests that one changes the bead weights from 81 to 85 g/mol , the bead diameters change from 5.1 to 5.4 \AA , while the required reduction of the bending stiffness decreases the Kuhn length in LJ units from $l_K = 2.19\sigma$ to $l_K = 2.07\sigma$. Compared to the dynamic effects discussed in the following section, it thus seems safe to transfer the $\beta\kappa$, M_b and σ values listed in Tab. II to other temperatures. This suggests that the *effective* bending rigidity at the KG-level appears is essentially entropic in origin, $\kappa_h \ll -T_{ref}\kappa_s$, and related to rotations between isomeric states [2]. Obviously, the relations provided above can be used to obtain an improved parameterization, if there is information available about the end-to-end distance and bulk density at the state point of interest.

E. Time mapping

To reproduce not only static but also dynamic properties of target systems, we require input on their Kuhn time, τ_K , or their effective viscosity, η_K , at the Kuhn scale. Equating with τ_K or η_K of the Kuhn mapped KG model, we can directly infer the value of the KG time unit τ in SI units from Eq. (13), since the value of $x = \beta\kappa(n_K)$ is known via Eq. (15) for the Kuhn number of the experimental system. However, to carry out this program, we

needed to overcome two difficulties.

While conceptually useful, τ_K and η_K are not straightforward to observe directly. Typically, one can extrapolate down to the Kuhn scale within a model, if there is information on (emergent) macroscopic behavior or time scales at some dynamic reference temperature, T_{ref}^{dyn} . In Section III we discuss suitable examples like the viscosity of unentangled chains, $\eta = n_K N_K \eta_K$, the entanglement time, $\tau_e = N_{eK}^2 \tau_K$, the Rouse time, $\tau_R = N_K^2 \tau_K$, or the terminal relaxation time, τ_{max} . Experimentally, the Kuhn time or equivalently the Kuhn friction can be obtained from neutron spin echo data [84] by applying expressions from Rouse theory to analyse the monomeric dynamics below the entanglement time scale as in our analysis of simulation data [66]. The entanglement time, τ_e , can be measured by oscillatory rheological experiments, dielectric relaxation and transverse relaxation NMR measurements, see e.g. Refs. [85–88]. We note that published estimates might be obtained by fitting data to expressions, which define these times using conventions for prefactors, which differ from those we have adopted here.

The second difficulty is the pronounced temperature dependence of the chain dynamics in polymer melts. Most commodity polymer melts become glassy below a temperature T_g in or slightly below the experimentally relevant temperature range. As a consequence, even a small change in temperature can have a significant impact on the dynamics. Experimentally, time-temperature superposition (TTS) [89] is used to explore polymer dynamics over a much wider range of frequencies than those directly accessible to a given measurement instrument. Here we use this approach to estimate the Kuhn time at the temperature of interest, T , given a Kuhn time measured at the reference temperature, T_{ref}^{dyn} :

$$\frac{\tau_K(T)}{\tau_K(T_{ref}^{dyn})} = a_T(T, T_{ref}^{dyn}) \quad (20)$$

As discussed in appendix A, the shift factor can be written as

$$\ln a_T(T, T_{ref}^{dyn}) = -\frac{C_{VF}(T - T_{ref}^{dyn})}{(T_{ref}^{dyn} - T_{VF})(T - T_{VF})} \quad (21)$$

Eq. (21) should be valid above the glass transition temperature in the temperature range $[T_g, T_g + 100K]$. Here we use a “universal” Vogel-Fulcher constant $C_{VF} = \ln(10) \times 17.44 \times 51.6K = 2072K$. Similarly, we set $T_{VF} = T_g - 51.6K$ for the Vogel-Fulcher temperature, where viscosities and associated time scales formally diverge. More detailed information and specific tables with fitted VF (or WLF, see appendix A) parameters can be found in Ref. [89].

The mapping relations for the temperature dependent conversion of the KG time τ resulting from Eq. (13) are shown in Tab. III and illustrated in Fig. 2. The converted values vary over a much wider range than the static parameters in Table II:

name	T_g [K]	T_{ref}^{dyn} [K]	τ_e^{exp} [s]	n_K	N_{eK}	$\tau_K(T_{ref}^{dyn})$ [ps]	$\eta_K(T_{ref}^{dyn})$ [mPa s]	$\tau(T_{ref}^{dyn})$ [ps]	$\sigma\sqrt{M_b/k_B T_{ref}^{dyn}}$ [ps]
PI-7	206	298	1.9×10^{-5}	2.72	42.55	3.9	61.5	2800	2.3
PDMS	150	298	1.1×10^{-7}	2.82	31.08	4.2	0.162	17	5.0
cis-PBd	174	298	8.8×10^{-8}	3.40	25.93	5.8	0.726	21	1.7
cis-PI	206	298	6.7×10^{-5}	3.47	17.1	6.0	424	17000	2.2
a-PP	262	348	1.9×10^{-6}	3.81	21.70	7.1	11.2	560	2.8
PIB	201	298	1.1×10^{-3}	3.94	19.52	7.5	4550	350000	4.0
a-PS	375	453	3.4×10^{-4}	4.54	18.35	9.5	1210	140000	6.8
PEO	210	348	1.5×10^{-8}	4.99	11.81	11	0.332	7	1.6

TABLE III: Parameters and characteristic times for commodity polymer melts and the corresponding KG models. The first set of numbers defines the experimental input: the experimental glass transition temperature and the dynamic reference temperature T_{ref}^{dyn} for the experimental entanglement time τ_e (and/or more suitable VF parameters). Using the static mapping and, in particular, the Kuhn number n_K , we can infer the number of Kuhn segments per entanglement length, N_{eK} , from Eq. (26) or more refined estimates [66, 77]. The Kuhn time, $\tau_K(T_{ref}^{dyn})$, and the viscosity at the Kuhn scale, $\eta_K(T_{ref}^{dyn})$, follow from Eqs. (5) and (30), the characteristic time scale, $\tau(T_{ref}^{dyn})$, of the corresponding Kuhn mapped KG model is given by Eq. (13). For comparison, we also list the estimate for τ that results from the static mapping. Finally, we can use Eqs. (20) and (21) to estimate τ_K , η_K , and τ over the entire TTS validity range (Fig. 2). References for experimental data: PI-7[78, 79], PDMS[80], cis-PDb[80], cis-PI[80], cis-PI[81], a-PP[82], and PEO [83].

PDMS, cis-PDb and PEO are experimentally studied about 150K above T_g , resulting in KG time scales in the 10ps range.

PI melts at 100K above T_g are represented by KG models with τ in the 10ns range.

PIB has a significantly higher $\tau \approx 350ns$ at a similar distance from the glass transition temperature. Perhaps this can be explained by specific intramolecular rotational barriers.[90].

a-PS has a comparable $\tau \approx 140ns$ at 80K above T_g , while

a-PP maps onto a KG model with $\tau \approx 0.6ns$ at a comparable distance from T_g

III. PREDICTING EMERGENT UNIVERSAL BEHAVIOR BEYOND THE KUHN SCALE

Having completed the matching of experimental systems and KG model polymer melts at the Kuhn scale, an obvious question arises: do we have reasons to believe, that this is “enough” to quantitatively describe the emergent behavior on much larger scales?

In the following, we provide a brief outline of polymer theory [3, 4, 70, 91] to argue that this is indeed the case. The point of the exercise is to illustrate, that two monodisperse polymer melts of chemically different polymers are expected to show the same universal large scale properties, provided (i) they are characterized by the same number of Kuhn segments per chain, N_K , (ii) the same dimensionless Kuhn number, n_K , and (iii) properties are measured in the “natural” Kuhn units. Our KG models can be expected to have predictive power for emergent polymer properties, if we may take it for

granted, that this universality of properties of different chemical species also extends to computational models that exhibit the key features of polymer melts: chain connectivity, local liquid-like monomer packing, and the impossibility of chain backbones to dynamically cross through each other.

We begin our short *tour d’horizon* with the Rouse model [3, 92], which describes the dynamics of short unentangled polymers. Rouse considered the Langevin dynamics of a “Gaussian” chain composed of beads, which experience local friction and which are connected by harmonic springs representing the entropic elasticity of polymer sections beyond the Kuhn scale. In this model, the maximal internal relaxation time of a chain is given by the Rouse time

$$\tau_R = N_K^2 \tau_K . \quad (22)$$

In the Rouse regime, the macroscopic melt viscosity can be written as

$$\eta = n_K N_K \eta_K . \quad (23)$$

The key for understanding the properties of polymer melts is the realisation, that chains strongly interpenetrate. The Flory number, $n_F = \rho_c \langle R^2 \rangle^{3/2}$, is defined as the number of chains populating, on average, the volume spanned by one chain. For our present purposes, it is important to note that n_F and hence the degree of this interpenetration can again be simply expressed as a sole function of the two dimensionless numbers characterising a melt on the Kuhn scale:

$$n_F = n_K N_K^{1/2} \quad (24)$$

or $n_F \sim 350$ for natural rubber.

That the Flory number is large, explains why chains behave nearly ideally in dense melts[93] and why such

polymer systems can often be well described by mean-field theories [94, 95]. *Beyond* the Kuhn scale, the universal aspects of mesoscale conformations[96, 97] and liquid structure[98, 99] in polymeric systems can be described by Gaussian chain models. In this model, the notion of a chain contour length is lost. This is particularly apparent in the continuum limit, which is frequently employed in theoretical calculations[3, 100]. Systems are thus characterised by a single dimensionless number, which is often referred to as the invariant degree of polymerization,

$$\bar{N} = \rho_c^2 \langle R^2 \rangle^3 = n_K^2 N_K = n_F^2. \quad (25)$$

This dimensionless measure plays a key role in more complex polymer systems such as block-copolymers undergoing micro phase separation[97, 101], since it is related to the number of intermolecular pair-interactions a given reference chain experiences. It is evident from Eq. (25) that Kuhn matched KG melts can be expected to automatically reproduce *all* emergent properties, which depend of the invariant degree of polymerization, \bar{N} . For a more detailed discussion of these aspects in the context of multi-scale modeling, we refer the reader to Refs. [102, 103]. In the following, we take a closer look a dynamic properties.

Chains undergoing Brownian motion can slide past each other, however, their backbones cannot cross[3]. As a consequence, the motion of long chains is subject to long-lived topological constraints[104]. Modern theories of polymer dynamics [3] are based on the idea that molecular entanglements confine individual chain segments to a one-dimensional, diffusive motion (reptation [105]) in tube-like regions in space [106]. The constraints become relevant at scales beyond the entanglement (contour) length[107, 108], L_e , or the equivalent number of Kuhn units between entanglements, $N_{eK} = L_e/l_K$. According to the packing argument for loosely entangled polymers [75, 109, 110], there are

$$N_{eK} = \left(\frac{\alpha}{n_K} \right)^2 \quad (26)$$

Kuhn segments per entanglement length. The corresponding spatial scale is the tube diameter which is given by

$$\frac{d_T}{l_K} = \sqrt{\frac{\langle R^2(N_{eK}) \rangle}{l_K^2}} = \sqrt{N_{eK}} = \frac{\alpha}{n_K} \quad (27)$$

To define a length scale characterizing the chain packing in a polymeric material, one can consider a spherical region centered on a chosen monomer. If the region is small, then most monomers found inside will belong to the same chain as the chosen monomer. If the region is large, then most monomers inside the region belong to other chains. The packing length [108, 111] is related to the Kuhn number as

$$\frac{p}{l_K} = \frac{V_c}{l_K \langle R^2 \rangle} = (l_K^3 \rho_K)^{-1} = n_K^{-1}, \quad (28)$$

The number of entanglement strands per entanglement volume is

$$\alpha = \frac{d_T}{p} = \frac{\rho_K}{N_{eK}} d_T^3 = 18 \pm 2, \quad (29)$$

which appears to be a universal constant for all flexible polymers [45, 109, 110, 112]. Values of α for the present polymer species are shown in Tab. I.

Just like the fundamental time scale τ_K is determined by Kuhn segment diffusion coefficient and the Kuhn length, the diffusion of an entanglement segment ($D_e = k_B T / [N_{eK} \zeta_K]$) and the tube diameter also define a characteristic time scale τ_e :

$$\frac{\tau_e}{\tau_K} = N_{eK}^2 = \left(\frac{\alpha}{n_K} \right)^4. \quad (30)$$

Above the entanglement time, the Rouse model fails to describe dynamic correlations in polymer melts. Again, the point to note is, that when defined in Kuhn units, the spatial and temporal scales that emerges due to entanglements only depend on the Kuhn number, n_K .

In the limit of long chains the maximal relaxation time is [105] is $\tau_{max} = 3Z^3 \tau_e$, where $Z = N_K / N_{eK}$ denotes the number of entanglements per chain. Using Eq. (26), we see that

$$Z = \frac{n_K^2 N_K}{\alpha^2} \quad (31)$$

only depends on dimensionless constants, which are reproduced in KG melts parameterized at the Kuhn scale. As a consequence, the correct number of entanglements emerges from the microscopic topological constraints in the KG melts, suggesting that they also exhibit the same asymptotic maximal relaxation time as the experimental target systems:

$$\frac{\tau_{max}}{\tau_K} = 3Z^3 \frac{\tau_e}{\tau_K} = 3 \frac{n_K^2 N_K^3}{\alpha^2}. \quad (32)$$

For chains of finite length, relaxation processes such as contour length fluctuations and constraint release modify the maximal relaxation time [3, 113]. But as such effects are controlled through the effective chain length, Z , in entanglement units, they can be also expected to be faithfully reproduced in our KG models [114].

Turning now to macroscopic material properties, in slowing down the chain equilibration after a deformation, entanglements dominate the viscoelastic behavior of high molecular weight polymeric liquids. For $\tau_e < t < \tau_{max}$ the shear relaxation modulus, $G(t)$ exhibits a rubber-elastic plateau, $G_N = \frac{4}{5} G_e$, where the entanglement modulus is[109, 110],

$$\frac{G_e l_K^3}{k_B T} = \frac{\rho_K l_K^3}{N_{eK}} = \frac{n_K^3}{\alpha^2}. \quad (33)$$

From the time dependent shear relaxation modulus one can obtain the shear compliance and the melt viscosity.

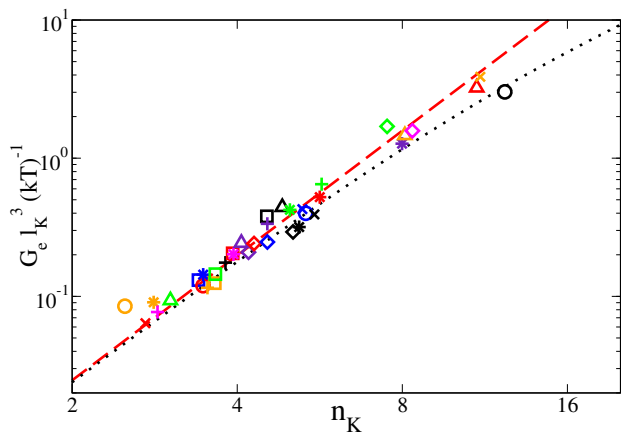


FIG. 3: Reduced entanglement moduli for the polymers in Tab. I compared to the theoretical expectation for flexible polymers eq. (33) (red dashed line) to our the semi-empirical prediction of eq. (42) in Ref. [66]) (black dotted line) The symbols denote in order of increasing Kuhn number: PI-50 (orange \circ), PI-7 (red \times), PDMS (orange $*$), PI-20 (magenta $+$), PI-34 (green Δ), cis-PBd (blue \square), PIB(413) (red \circ), cis-PI (blue $*$), a-PP(463) (orange $+$), i-PP (orange \square), a-PP(413) (green \square), a-PP(348) (black $+$), a-PP (red \square), PIB (magenta $*$), a-PMMA (indigo Δ), i-PS (indigo \diamond), a-PMA (red \diamond), PI-75 (black \square), PBd-20 (indigo $+$), a-PS (blue \diamond), PBd-98 (black Δ), PEO (green $*$), POM (black \diamond), a-PHMA (black $*$), a-PVA (blue \times), SBR (blue \circ), P6N (black \times), h a-PAMS (red $*$), a-PEA (green $+$), PET (green \diamond), s-PP (indigo $*$), PE(413) (orange Δ), a-POA (magenta \diamond), PC (red Δ), PE (orange \times), and PTFE (black \circ).

The asymptotically expected result [3] for long entangled chains is given by

$$\frac{\eta}{\eta_K} = \frac{\pi^2}{15} \frac{G_e \tau_{max}}{\eta_K} = \frac{12}{5} \frac{n_K^5 N_K^3}{\alpha^4}. \quad (34)$$

suggesting that this property should also be quantitatively reproduced by our KG models.

Figure 3 shows the reduced entanglement moduli as a function of Kuhn number. The experimental data are in good agreement with eq. (33) for flexible chains.[112] The scatter observed between the experimental plateau moduli and the predicted plateau modulus line must be attributed either to chemical details causing some small degree of non-universal behaviour[115], such as a non-negligible crystalline fraction, or to experimental uncertainties in accurately estimating the plateau modulus which can be quite difficult.[116] For the very largest Kuhn numbers, the experimental data points can not discriminate between the packing argument and the predicted cross-over to the tightly entangled regime.[66, 75]

Figure 4 shows a comparison between experimental plateau moduli and entanglement moduli of KG melts extracted from Primitive Path Analysis [66, 114]. Most of the experimental values are within the 25% error interval around the line defined by the one parameter KG models. This is concrete evidence, that the emergent en-

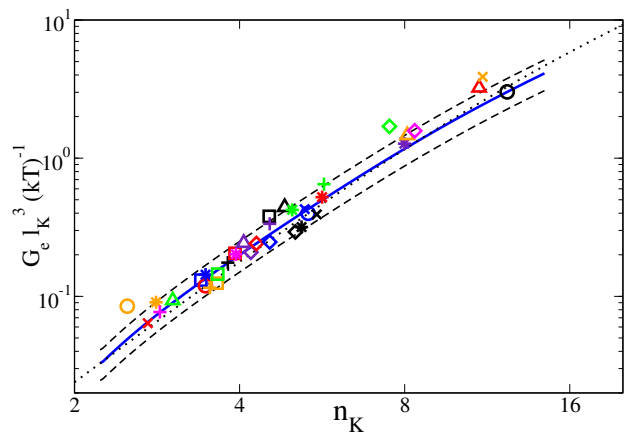


FIG. 4: Reduced entanglement moduli for the experimental data in Fig. 3 compared to the range of KG models for $-1 \leq \beta\kappa \leq 2.5$ (blue solid line), with indications of $\pm 25\%$ error (dashed black lines). Also shown are our the semi-empirical prediction of eq. (42) in Ref. [66]) (black dotted line)

tanglement properties of our KG models agree with those of the targeted experimental polymer systems. Interestingly, the stiffer KG models also seem to be in excellent agreement with the predicted cross-over to tightly entangled regime.[66, 75]

To summarise: we have illustrated how static, dynamic, mesoscopic and macroscopic properties of polymer melts depend on just two dimensionless parameters: the Kuhn number and the number of Kuhn segments per chain length when these properties are expressed in natural dimensionless form using the Kuhn length, Kuhn time, Kuhn viscosity and the thermal excitation energy. Hence we expect to obtain identical dimensionless results from experiments of chemical polymer systems and from simulations of model polymer systems when the Kuhn number and number of Kuhn units per chain used in the KG model simulations match those of the polymer species.

IV. DISCUSSION

Polymeric systems exhibit a wide range of characteristic time and length scales. This is readily illustrated for the example of natural rubber, i.e. melts of *cis*-PI chains with a typical length of $N_K = 10^4$ Kuhn segments. Important characteristic length scales comprise (i) the Kuhn length, $l_K \approx 1nm$, (ii) the tube diameter, $d_T \approx 5nm$, (iii) the coil diameter, $\langle R^2 \rangle \approx 100nm$, and (iv) the contour length, $L \approx 10\mu m$. The spread is even larger between the characteristic time scales. There are already almost three orders of magnitude between the Kuhn time, $\tau_K \sim 1 \times 10^{-7}s$, and the entanglement time, $\tau_K \sim 7 \times 10^{-5}s$. The Rouse time of $\tau_R \sim 10^8 \tau_K \sim 10s$ governs *fast* processes such as the tension equilibration inside the tube [3], while the estimated disentanglement

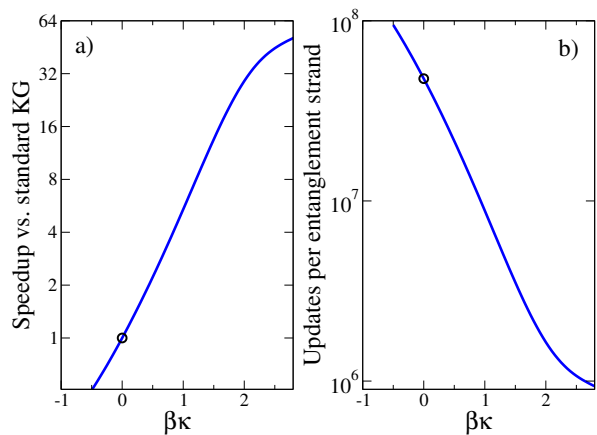


FIG. 5: Speed up of KG models due to increased stiffness. The left graph shows the speed up relative to the standard KG model with $\beta\kappa = 0$, while the right graph shows the number of particle updates, $N_{eb} \frac{\tau_e}{\delta t}$, required to follow the dynamics of one entanglement strand over the entanglement time.

time is $\tau_{max} \sim 4h$.

The slow dynamics has dramatic consequences for macroscopic properties such as the viscosity. Our estimate of the effective viscosity at the Kuhn scale is $\eta_K \approx 0.4 Pa s$. The viscosity of a short chain melt at the entanglement threshold, $N_K = N_{eK}$, is already two orders of magnitude larger, $\eta_e \approx 40 Pa s$, while for our strongly entangled ($Z = N_K/N_{eK} = 400$) example, $\eta \approx 5 \times 10^9 Pa s$. In other words, the long chain melt exhibits a *macroscopic* viscosity similar to glass forming liquids close to T_g , even though locally the chains experience a friction as if they were immersed in motor oil.

The wide range of relevant time and length scales in polymeric systems makes them natural targets for multi-scale modelling.[13, 117, 118] In particle-based models, the resolution ranges from the atom scale to DPD-like descriptions, where entire chains are represented by one or two soft spheres or ellipsoids[102, 119]. What is the natural place of KG-like models in this hierarchy? And how should they be parameterized?

A. Entanglement vs. Kuhn scale as targets for KG models

Typically, the KG model is mapped to experiments [8, 62] or simulations of more microscopic models [120] on the entanglement scale. Inspections of the formulas in Sec. III suggests, that one can hope to reproduce the large scale dynamics by matching the number of entanglements, Z , between target and model system and by identifying the tube diameter, d_T , as the unit of spatial distance as well as the entanglement time, τ_e , as the unit of time. Conceptually, this is what universality is all about and not different from using experimental data for PDMS to predict universal aspects of the behavior of,

say, amorphous polystyrene.

As illustrated by Fig. 5, it is tempting to use the additional stiffness parameter [64] to reduce the CPU time required to reach the entanglement scale [44, 65]. But how far up the scales can one safely push characteristic features of the KG model like the well-defined, almost inextensible contour length and the almost fully excluded molecular volume? These features are adequate for a description on the Kuhn scale, but not for a generic model of loosely entangled chains at the entanglement scale.

Targeting the Kuhn scale, as we advocate here, provides a simple physical motivation for the choice of the stiffness parameter and should help to reduce “gaps” [120] relative to predictions of more microscopic models for the local behavior. Since $\beta\kappa > 0$ for most Kuhn matched KG models of commodity polymers, they are *more* efficient than the original KG model in reaching the entanglement scale, even though by targeting the Kuhn scale the models are nominally more microscopic. Typical speedups are of the order of 4, in the case of polycarbonate they reach a factor of 30 (Fig. 5).

B. Linear vs. nonlinear universality in the rheology of polymer melts

Crucially, we can hope to extend the validity range of the KG model by, to paraphrase Einstein, making the chains “as stiff as possible, but not stiffer.” By reproducing the number of Kuhn segments per entanglement length, N_{eK} , the models account for the maximal chain extension, $\sqrt{N_{eK}}$, under strong deformations. Furthermore, KG melts parameterized at the Kuhn scale plausibly exhibit friction reduction in fast elongational flows, in so far as the effect can be attributed to the alignment of the Kuhn segments to the stretching direction[121, 122]. There are thus good reasons to expect, that the models discussed in the present article fulfil all *three* conditions for *non-linear* universality in the rheology of polymer melts [123].

C. Computational performance of Kuhn matched KG models compared to descriptions on neighboring scales

Kuhn matched KG models are computationally much less demanding than atomistic simulations. This is due to two factors: (i) There is a considerable reduction in the number of degrees of freedom. We have not counted atoms, but assuming carbon and hydrogen atoms as the dominant components, molecular bead weights between $40g/mol$ and $700g/mol$ translate to 3 to 50 united atoms that are being represented by one KG bead. If hydrogen atoms are represented explicitly, then these numbers increase by an additional factor of two or three. (ii) At the reference temperature, T_{ref}^{dyn} , of the rheological exper-

iments, our estimates for the physical meaning of the KG unit of time, τ , vary in the range $5ps < \tau < 0.35\mu s$. The corresponding time step of $50fs < \delta t = 10^{-2}\tau < 3.5ns$ is thus 50 to 3.5×10^6 times larger than the $1fs$ time step in atomistic simulations. The time step in atomistic simulations is dictated by typical frequency of bond vibrations. Whereas if bond lengths are constrained, then the typical time scale is that of bond angle vibrations which occurs on time scales of tens of fs . [117, 124] For systems closer to the glass transition, the speedup in modelling the large scale behaviour along the present lines would be exponentially larger. Compared to an atomistic model, this obviously comes at the price of loosing the ability to *predict* any of the glassy behaviour.

With at least 10^6 particle updates per entanglement strand and time (inset Fig. 5), Kuhn matched KG models are bound to be slower than PPA-parameterized slip-link augmented DPD-models [125–129]. Again, the more coarse-grain description benefits from a reduction of the number of degrees of freedom by a factor of the order of $1/N_{eK}$ as well as a corresponding reduction of the number of time steps by a factor of $\tau_K/\tau_e \sim 1/N_{eK}^2$. For the intrinsically most flexible polymers in Table I, the speedups may be as large as a factor of 10^4 or even 10^5 in rare cases. While this approach is clearly successful, there is nevertheless a price to be paid: effects of topological constraints do not *emerge* through the same mechanisms as in the target systems, but are described within a phenomenological model. While the tube/slip-link model is in general well understood [116], we suspect that non-linear universality [123] or the emergence of crumpling in non-concatenated ring melts [44, 45] remain a challenge.

D. Kuhn scale matching as a special case of structure based coarse-graining

The construction of coarse-grain models requires choices and the definition of (subjective) priorities. A classic example is the tension between structure-based approaches [6, 7, 13] and schemes focused on preserving thermodynamic properties [130].

Kuhn scale matching can be viewed as a special case of structure-based coarse-graining. It is guided by theoretical considerations, which identify the Kuhn scale as controlling the emergent, universal behavior at larger time and length scales. Consequently, no particular effort is made to reproduce the local behavior. The resulting “one parameter force-field” for the KG model is remarkably simple, but this simplicity obviously comes at the price of loosing the ability to predict (or to understand) the behaviour of experimental target systems below the Kuhn scale. In particular, this holds on the bead scale, where we employ a computationally convenient, generic model without any particular relation to the properties (or the structure) of the target system.

The techniques for structure-based coarse-graining are well understood [10, 131–133]. If applied on a similar level

of coarse-graining as our KG models (i.e. retaining a comparable number of degrees of freedom), the resulting models can be expected to offer a locally more faithful representation. The differences are probably minor for polymers like isotactic polystyrene, where our KG beads represent three polystyrene monomers. The situation is different for polymers like polycarbonate, whose monomers are represented by several KG beads. There is no reason whatsoever, why the “beads” arising from systematic coarse-graining ought to be of equal size, spherical or be joined in a straight line like those of our KG models. [10, 28, 119] Such models may provide insight into the relation between structure, local dynamics, and the dissipation mechanisms responsible for the glassy dynamics, which is lost in our approach. In terms of computational performance, they should fall in between atomistic descriptions and Kuhn matched KG models, since they need to resolve motion on smaller time scales.

E. Time scales in coarse-grain models

There is a persistent idea in the literature [8] that the time scale in simulations of coarse-grain models can be inferred by standard dimensional analysis. The difficulty becomes clear, if we try to follow this approach on the Kuhn scale. The time scale $l_K \sqrt{M_K/k_B T}$ can be understood as the time required by a Kuhn segment to ballistically cover a distance comparable to its size, l_K , if it moves at its thermal velocity, $v_K^{th} = \sqrt{k_B T/M_K}$. In contrast, the physically relevant Kuhn time, τ_K , is controlled by the local viscosity, Eq. (4), which emerges from microscopic interactions below the Kuhn scale and which is expected to display an exponential WLF temperature dependence, Eqs. (20) and (21).

The systematic linking of times scales on different levels of spatial and temporal resolution remains a challenge. A conceptual framework is provided by the Mori-Zwanzig projector formalism. [134, 135] Here the projection operator is defined by the choice of “slow” CG variables. The formalism provides a generalized Langevin equation (GLE) for the time evolution of the CG variables, where the effect of the “fast” variables is described by the GLE memory kernel giving rise to friction and stochastic forces applied to the slow variables. In practice, sampling such GLE memory kernels requires simulations of the fast dynamics for fixed slow variables, which is complicated and has only been achieved relatively recently. [136–138]

In practice [24], one often uses a mapping approach, where the time scale of the coarse-grain simulations is determined by the condition, that the coarse-grain and the microscopic model predict identical dynamics on the largest time scales accessible to the microscopic approach. In the present case, we have used a mapping on the Kuhn scale to estimate the physical meaning of the KG time scale τ . As shown in Table III and Figure 2, these estimates exceed by orders of magnitude the time scale arising from the standard combination $\sigma \sqrt{M_b}/\epsilon$ of

the diameter and mass M_b of the KG beads with the energy scale of the model.

This mismatch strikes us as a natural and highly desired consequence of the elimination of microscopic degrees of freedom and of the associated dissipation mechanisms. In principle, it is possible to preserve $\sigma\sqrt{M_b/\epsilon}$ as the definition of time by tuning the friction of a Langevin (or preferentially, DPD[139]) thermostat such that the resulting τ_K matches the experimental target value. However, this would make the simulations orders of magnitude more expensive in terms of computer time without providing additional physical insight.

F. Kuhn scale matched KG models as part of a multiscale hierarchy of polymer polymers

In our opinion, the Kuhn scale merits to be systematically included in the hierarchy of multi-scale models of polymeric systems. Omitting it risks to mask a remarkable simplicity, which emerges from the universality of polymeric behavior.

We have focused on the KG model with bending rigidity, because it has been used in a vast number of publications as a basis for studying generic polymer and materials physics, see e.g. [6, 7, 13] for reviews. Furthermore, there are several fast equilibration procedures [103, 140, 141], which allow to build very well equilibrated, highly entangled melt configurations at relatively low computational cost. Obviously, one could apply the same logic to bead-spring models with variable density, to models based on chains of rods rather than beads[142] or to lattice models[143–146] as long as these capture the relevant physics of polymers.

Kuhn matched polymer models are easy to connect to neighboring scales. In the “up”-direction, the primitive path analysis [147] provides a systematic link to phenomenological models describing polymers on the entanglement scale[125–129]. In the “down” direction, they enable the generation of well equilibrated atomistic material models through fine-graining of melt configurations of a chemistry-specific KG model.[148]

The information we used here to parameterize the KG model was obtained *top-down* from experiment[74]. Our aim was to provide reasonable estimates of these parameters for a wide variety of polymer species and over the entire experimentally relevant temperature range. Alternatively, one could analyse simulations of atomistic [15–21, 21–27, 31, 32] or mildly coarse-grain [28–30] models of target polymers at specific state points. If the purpose is solely to parameterize the present model, then it suffices to analyze the simulations along the lines of the accompanying paper [66]. The inferred Kuhn length, density and time are straightforward to convert into a *bottom-up* parameterization of the KG model, which then provides access to much larger time and length scales than the original, more microscopic model.

V. CONCLUSION

We have argued that the Kuhn scale is a natural scale (i) to link theories, experiments and simulations of amorphous polymer melts and (ii) to target in building computational polymer models. Omitting the Kuhn scale from the hierarchy of multi-scale models risks to mask a remarkable simplicity, which emerges from the universality of polymeric behavior.

In practical terms, we have shown how to model homopolymer melts of a large variety of polymer species with an extension of the Kremer-Grest model [61, 62], which was originally introduced by Faller and Müller-Plathe [63]. The force field has a single adjustable parameter, the chain stiffness. We determine this parameter by matching the (Kuhn) number of Kuhn segments per Kuhn volume, $n_K = \rho_K l_K^3$, of the target polymer species and the KG polymer model. No attempt is made to reproduce smaller scale features. Besides expressions for estimating the model parameters from experimental input, we have provided tables listing which bending stiffness to use for particular polymer species and how to translate KG into SI units. Our estimates for the mapping from simulation to physical time are based on time-temperature superposition.

Conceptually, Kuhn scale matching can be seen as a special case of structure based coarse-graining. The choice of the structural features to be preserved is guided by theoretical considerations, which identify the Kuhn scale as controlling the emergent universal polymer behavior at larger time and length scales.

The resulting coarse-graining level is about one bead per chemical monomer or two to three beads per Kuhn segment. Kuhn matched KG models thus fall in between atomistic or mildly coarse-grain models and descriptions on the entanglement scale. Both coarse-graining steps, from the atom to the Kuhn and from the Kuhn to the entanglement scale, are associated with performance gains of several orders of magnitude. For systems close to the glass transition, the speedup in modelling the large scale behaviour is even exponentially larger. Compared to atomistic descriptions, Kuhn matched KG models lose the ability to predict the microscopic (glassy) dynamics or to reproduce semi-crystalline ordering. Compared to phenomenological entanglement models, Kuhn matched KG models preserve the emergence of the full spectrum of universal amorphous polymer properties through the same mechanisms as in the experimental target systems. In particular, we expect them to automatically fulfil all *three* conditions for non-linear universality in the rheology of polymer melts [123].

An interesting challenge for future work would be the parameterization of a corresponding force-field for copolymer systems, using for example the technique from Ref. [149]. While this should, in principle, be possible at least for static properties, modelling the dynamics might no longer be as simple as adjusting a single time scale. Similarly, it might be possible to parameterise minimal

models of glassy[150, 151] or semi-crystalline[67] polymers along the present lines.

Appendix A: Time-temperature superposition

For a TTS reference temperature T_0 the empirical Williams-Landel-Ferry (WLF)[152] shift factor has the form

$$\log_{10} a_T(T; T_0) = -\frac{C_1(T_0)(T - T_0)}{C_2(T_0) + (T - T_0)}. \quad (\text{A1})$$

Eq. (A1) is valid above the glass transition temperature in the temperature range $[T_g, T_g + 100K]$. Using T_g as reference temperature, the constants adopt “universal” values $C_1^g \approx 15$ and $C_2^g \approx 50K$. [152] Other choices require suitably adjusted parameters $C_1(T_0)$ and $C_2(T_0)$.

The conversion can be avoided by writing the shift factor in a form derived from the equivalent Vogel-Fulcher-Tammann-Hesse equation [Refs. 14-16 from Ngai]

$$\ln a_T(T; T_0) = -\frac{C_{VF}(T - T_0)}{(T_0 - T_{VF})(T - T_{VF})}. \quad (\text{A2})$$

The relations

$$T_{VF} = T_0 - C_2(T_0) \quad (\text{A3})$$

$$\Leftrightarrow C_2(T_0) = T_0 - T_{VF}$$

$$C_{VF} = \ln(10)C_1(T_0)C_2(T_0) \quad (\text{A4})$$

$$\Leftrightarrow C_1(T_0) = \frac{C_{VF}}{\ln(10)(T_0 - T_{VF})}$$

with $C_{VF} \approx 2000K$ allow to pass between the two representations. In particular, Eqs. (A1) and (A2) suggests (i) that the viscosity diverges at the Vogel-Fulcher temperature $T_{VF} = T_g - C_2^g$ located $\sim 50K$ below the glass transition temperature and (ii) that the orders of magnitude by which the viscosity drops in the opposite limit of $T \rightarrow \infty$ are given by $C_1(T_0)$ and are hence inversely proportional to the distance of the reference from the Vogel-Fulcher temperature. More detailed information and specific tables can be found in Ref. [89]. Note, however, that their Eq. (26.3) ought to read

$$\log_{10} a_T(T; T_0) = \frac{C_{VF}/\ln(10)}{T - T_{VF}} - \frac{C_{VF}/\ln(10)}{T_0 - T_{VF}}. \quad (\text{A5})$$

-
- [1] P. J. Flory, *Principles of polymer chemistry* (Cornell University Press, Ithaca N.Y, 1953).
- [2] P. Flory and M. Volkenstein, *Statistical mechanics of chain molecules* (1969).
- [3] M. Doi and S. F. Edwards, *The Theory of Polymer Dynamics* (Clarendon, Oxford, 1986).
- [4] P. G. de Gennes, *Scaling Concepts in Polymer Physics* (Cornell University Press, Ithaca NY, 1979).
- [5] K. Binder, *Monte Carlo and Molecular Dynamics simulations in polymer science* (Oxford University Press: New York, 1995).
- [6] K. Kremer, in *Soft and fragile matter: Non equilibrium dynamics, metastability and flow*, edited by M. E. Cates and M. R. Evans (J. W. Arrowsmith Ltd., Bristol, U.K., 2000), p. 145.
- [7] K. Kremer, *Macromol. Chem. Phys.* **204**, 257 (2003).
- [8] M. Kröger, *Phys. Rep.* **390**, 453 (2004).
- [9] F. Müller-Plathe, *Soft Mater.* **1**, 1 (2002).
- [10] F. Müller-Plathe, *Chem. Phys. Chem.* **3**, 754 (2002).
- [11] Q. Sun and R. Faller, *Comput. Chem. Eng.* **29**, 2380 (2005).
- [12] C. Tzoumanekas and D. N. Theodorou, *Curr. Opin. Solid State Mater. Sci.* **10**, 61 (2006).
- [13] C. Peter and K. Kremer, *Soft Matter* **5**, 4357 (2009).
- [14] Y. Li, B. C. Abberton, M. Kröger, and W. K. Liu, *Polymers* **5**, 751 (2013).
- [15] J. Padding and W. Briels, *J. Chem. Phys.* **117**, 925 (2002).
- [16] L. Liu, J. Padding, W. den Otter, and W. Briels, *J. Chem. Phys.* **138**, 244912 (2013).
- [17] K. M. Salerno, A. Agrawal, D. Perahia, and G. S. Grest, *Phys. Rev. Lett.* **116**, 058302 (2016).
- [18] R. Faller and F. Müller-Plathe, *Polymer* **43**, 621 (2002).
- [19] R. Faller and D. Reith, *Macromolecules* **36**, 5406 (2003).
- [20] Y. Li, M. Kröger, and W. K. Liu, *Polymer* **52**, 5867 (2011).
- [21] G. Maurel, F. Goujon, B. Schnell, and P. Malfreyt, *RSC Adv.* **5**, 14065 (2015).
- [22] V. Harmandaris, N. Adhikari, N. F. van der Vegt, and K. Kremer, *Macromolecules* **39**, 6708 (2006).
- [23] X. Chen, P. Carbone, W. L. Cavalcanti, G. Milano, and F. Müller-Plathe, *Macromolecules* **40**, 8087 (2007).
- [24] D. Fritz, K. Koschke, V. A. Harmandaris, N. F. van der Vegt, and K. Kremer, *Phys. Chem. Chem. Phys.* **13**, 10412 (2011).
- [25] H. A. Karimi-Varzaneh, P. Carbone, and F. Müller-Plathe, *J. Chem. Phys.* **129**, 154904 (2008).
- [26] H. Eslami, H. A. Karimi-Varzaneh, and F. Müller-Plathe, *Macromolecules* **44**, 3117 (2011).
- [27] C. Chen, P. Depa, J. K. Maranas, and V. G. Sakai, *J.*

- Chem. Phys. **128**, 124906 (2008).
- [28] W. Tschöp, K. Kremer, J. Batoulis, T. Bürger, and O. Hahn, *Acta. Polym.* **49**, 61 (1998).
- [29] C. F. Abrams and K. Kremer, *Macromolecules* **36**, 260 (2003).
- [30] B. Hess, S. León, N. Van Der Vegt, and K. Kremer, *Soft Matter* **2**, 409 (2006).
- [31] T. Strauch, L. Yelash, and W. Paul, *Phys. Chem. Chem. Phys.* **11**, 1942 (2009).
- [32] G. Milano and F. Müller-Plathe, *J. Phys. Chem. B.* **109**, 18609 (2005).
- [33] J. Baschnagel, K. Binder, P. Doruker, A. A. Gusev, O. Hahn, K. Kremer, W. L. Mattice, F. Müller-Plathe, M. Murat, and W. Paul, in *Viscoelasticity, atomistic models, statistical chemistry* (Springer, 2000), p. 41.
- [34] P. Carbone, H. A. K. Varzaneh, X. Chen, and F. Müller-Plathe, *J. Chem. Phys.* **128**, 064904 (2008).
- [35] M. E. Johnson, T. Head-Gordon, and A. A. Louis, *J. Chem. Phys.* **126**, 144509 (2007).
- [36] S. K. Sukumaran, G. S. Grest, K. Kremer, and R. Everaers, *J. Polym. Sci., Part B: Polym. Phys.* **43**, 917 (2005).
- [37] W. W. Graessley, *Adv. Polym. Sci.* **47**, 67 (1982).
- [38] G. Marrucci, *J. Polym. Sci., Polym. Phys. Ed.* **23**, 159 (1985).
- [39] M. Rubinstein and R. H. Colby, *J. Chem. Phys.* **89**, 5291 (1988).
- [40] G. Marrucci and G. Ianniruberto, *Phil. Trans. R. Soc. Lond. A* **361**, 677 (2003).
- [41] G. Ianniruberto and G. Marrucci, *J. Rheol.* **58**, 89 (2014).
- [42] A. Rosa and R. Everaers, *PLoS. Comput. Biol.* **4**, e1000153 (2008).
- [43] J. D. Halverson, G. S. Grest, A. Y. Grosberg, and K. Kremer, *Phys. Rev. Lett.* **108**, 038301 (2012).
- [44] J. D. Halverson, W. B. Lee, G. S. Grest, A. Y. Grosberg, and K. Kremer, *J. Chem. Phys.* **134**, 204904 (2011).
- [45] A. Rosa and R. Everaers, *Phys. Rev. Lett.* **112**, 118302 (2014).
- [46] J. P. Wittmer, H. Meyer, J. Baschnagel, A. Johner, S. Obukhov, L. Mattioni, M. Müller, and A. N. Semenov, *Phys. Rev. Lett.* **93**, 147801 (2004).
- [47] G. S. Grest, K. Kremer, S. T. Milner, and T. A. Witten, *Macromolecules* **22**, 1904 (1989).
- [48] G. S. Grest and K. Kremer, *Macromolecules* **23**, 4994 (1990).
- [49] E. R. Duering, K. Kremer, and G. S. Grest, *Phys. Rev. Lett.* **67**, 3531 (1991).
- [50] C. Svaneborg, G. S. Grest, and R. Everaers, *Phys. Rev. Lett.* **93**, 257801 (2004).
- [51] C. Svaneborg, R. Everaers, G. S. Grest, and J. G. Curro, *Macromolecules* **41**, 4920 (2008).
- [52] T. Aoyagi, J.-I. Takimoto, and M. Doi, *J. Chem. Phys.* **115**, 552 (2001).
- [53] F. Pierce, D. Perahia, and G. S. Grest, *Macromolecules* **42**, 7969 (2009).
- [54] M. Murat and G. S. Grest, *Macromolecules* **24**, 704 (1991).
- [55] M. Murat and G. S. Grest, *Phys. Rev. Lett.* **63**, 1074 (1989).
- [56] G. S. Grest, *Phys. Rev. Lett.* **76**, 4979 (1996).
- [57] H. Yagyu and T. Utsumi, *Comput. Mater. Sci.* **46**, 286 (2009).
- [58] D. M. Sussman, W.-S. Tung, K. I. Winey, K. S. Schweizer, and R. A. Riggleman, *Macromolecules* **47**, 6462 (2014).
- [59] D. Gersappe, *Phys. Rev. Lett.* **89**, 058301 (2002).
- [60] T. Ge, M. O. Robbins, D. Perahia, and G. S. Grest, *Phys. Rev. E.* **90**, 012602 (2014).
- [61] G. S. Grest and K. Kremer, *Phys. Rev. A* **33**, 3628 (1986).
- [62] K. Kremer and G. S. Grest, *J. Chem. Phys.* **92**, 5057 (1990).
- [63] R. Faller, A. Kolb, and F. Müller-Plathe, *Phys. Chem. Chem. Phys.* **1**, 2071 (1999).
- [64] R. Faller, F. Müller-Plathe, and A. Heuer, *Macromolecules* **33**, 6602 (2000).
- [65] R. Faller and F. Müller-Plathe, *Chem. Phys. Chem.* **2**, 180 (2001).
- [66] C. Svaneborg and R. Everaers, *Characteristic time and length scales in kremer-grest bead-spring polymer melts as a function of chain stiffness. Manuscript submitted to Macromolecules.* (2018).
- [67] H. Meyer and F. Müller-Plathe, *The Journal of Chemical Physics* **115**, 7807 (2001).
- [68] R. S. Hoy and N. C. Karayiannis, *Phys. Rev. E* **88**, 012601 (2013).
- [69] J. Morthomas, C. Fusco, Z. Zhai, O. Lame, and M. Perez, *Phys. Rev. E.* **96**, 052502 (2017).
- [70] M. Rubinstein and R. H. Colby, *Polymer physics* (Oxford University, New York, 2003).
- [71] W. Kuhn, *Kolloid.* **1**, 2 (1934).
- [72] O. Kratky and G. Porod, *Rec. Trav. Chim.* **1106**, 2211 (1949).
- [73] Y. Ding and A. P. Sokolov, *Macromolecules* **39**, 3322 (2006).
- [74] L. J. Fetters, D. J. Lohse, and R. H. Colby, in *Physical properties of polymers handbook*, edited by J. Mark (Springer, 2007), p. 447.
- [75] N. Uchida, G. S. Grest, and R. Everaers, *J. Chem. Phys.* **128**, 044902 (2008).
- [76] S. Meyer, D. Jost, N. Theodorakopoulos, M. Peyrard, R. Lavery, and R. Everaers, *Biophys. J.* **105**, 1904 (2013).
- [77] N. Uchida, G. S. Grest, and R. Everaers, *J. Chem. Phys.* **128**, 044902 (2008).
- [78] J. T. Gotro and W. W. Graessley, *Macromolecules* **17**, 2767 (1984).
- [79] M. Abdel-Goad, W. Pyckhout-Hintzen, S. Kahle, J. Allgaier, D. Richter, and L. J. Fetters, *Macromolecules* **37**, 8135 (2004).
- [80] F. Vaca Chávez and K. Saalwächter, *Macromolecules* **44**, 1549 (2011).
- [81] D. Auhl, J. Ramirez, A. E. Likhtman, P. Chambon, and C. Fernyhough, *J. Rheol.* **52**, 801 (2008).
- [82] J. van Meerveld, *Rheol. Acta.* **43**, 615 (2004).
- [83] K. Niedzwiedz, A. Wischniewski, W. Pyckhout-Hintzen, J. Allgaier, D. Richter, and A. Faraone, *Macromolecules* **41**, 4866 (2008).
- [84] D. Richter, M. Monkenbusch, A. Arbe, and J. Colmenero, *Neutron spin echo in polymer systems* (Springer, 2005).
- [85] R. B. Bird, R. C. Armstrong, and O. Hassager, *Dynamics of Polymeric Liquids*, vol. 1 (Wiley, New York, 1977).
- [86] H. Watanabe, *Prog. Polym. Sci.* **24**, 1253 (1999).
- [87] T. C. B. McLeish, *Adv. Phys.* **5**, 1379 (2002).
- [88] K. Saalwächter, *Prog. Nucl. Magn. Reson. Spectrosc.*

- 51**, 1 (2007).
- [89] K. L. Ngai and D. J. Plazek, in *Physical Properties of Polymers Handbook* (Springer, 2007), p. 455.
- [90] A. Arbe, M. Monkenbusch, J. Stellbrink, D. Richter, B. Farago, K. Almdal, and R. Faust, *Macromolecules* **34**, 1281 (2001).
- [91] A. R. Khokhlov, A. Y. Grosberg, and V. S. Pande, *Statistical Physics of Macromolecules* (AIP-Press, Jericho NY, 1994).
- [92] P. E. Rouse, *J. Chem. Phys.* **21**, 1272 (1953).
- [93] P. J. Flory, *J. Chem. Phys.* **17**, 303 (1949).
- [94] F. Schmid, *J. Phys. Cond. Matter* **10**, 8105 (1998).
- [95] M. Müller and F. Schmid, in *Advanced Computer Simulation Approaches for Soft Matter Sciences II* (Springer, 2005), p. 1.
- [96] J. P. Wittmer, P. Beckrich, H. Meyer, A. Cavallo, A. Johner, and J. Baschnagel, *Phys. Rev. E* **76**, 011803 (2007).
- [97] J. Glaser, J. Qin, P. Medapuram, and D. C. Morse, *Macromolecules* **47**, 851 (2014).
- [98] M. Müller and K. Binder, *Macromolecules* **28**, 1825 (1995).
- [99] A. Clark, J. McCarty, and M. Guenza, *J. Chem. Phys.* **139**, 124906 (2013).
- [100] K. F. Freed, *"Renormalization Group Theory of Macromolecules."* (Wiley Interscience, New York, 1987).
- [101] G. H. Fredrickson and E. Helfand, *J. Chem. Phys.* **87**, 697 (1987).
- [102] M. Müller, in *Hybrid Particle-Continuum Methods in Computational Materials Physics*, edited by M. H. Müser, G. Sutmann, and R. G. Winkler (Forschungszentrum Jülich, 2013), vol. 46, p. 127.
- [103] G. Zhang, T. Stuehn, K. C. Daoulas, and K. Kremer, *J. Chem. Phys.* **142**, 221102 (2015).
- [104] S. F. Edwards, *Proc. Phys. Soc.* **91**, 513 (1967).
- [105] P. G. de Gennes, *J. Chem. Phys.* **55**, 572 (1971).
- [106] S. F. Edwards, *Proc. Phys. Soc.* **92**, 9 (1967).
- [107] L. J. Fetters, D. J. Lohse, and W. W. Graessley, *J. Polym. Sci., Part B: Polym. Phys.* **37**, 1023 (1999).
- [108] L. J. Fetters, D. J. Lohse, S. T. Milner, and W. W. Graessley, *Macromolecules* **32**, 6847 (1999).
- [109] Y.-H. Lin, *Macromolecules* **20**, 3080 (1987).
- [110] T. A. Kavassalis and J. Noolandi, *Phys. Rev. Lett.* **59**, 2674 (1987).
- [111] T. A. Witten, S. T. Milner, and Z.-G. Wang, in *Multiphase macromolecular systems*, edited by B. Culbertson (Plenum Press, New York, 1989), p. 655.
- [112] L. J. Fetters, D. J. Lohse, D. Richter, T. A. Witten, and A. Zirkel, *Macromolecules* **27**, 4639 (1994).
- [113] A. E. Likhtman and T. C. McLeish, *Macromolecules* **35**, 6332 (2002).
- [114] J.-X. Hou, C. Svaneborg, R. Everaers, and G. S. Grest, *Phys. Rev. Lett.* **105**, 068301 (2010).
- [115] H. J. Unidad, M. A. Goad, A. R. Bras, M. Zamponi, R. Faust, J. Allgaier, W. Pyckhout-Hintzen, A. Wischniewski, D. Richter, and L. J. Fetters, *Macromolecules* **48**, 6638 (2015).
- [116] A. Likhtman and T. McLeish, *Macromolecules* **35**, 6332 (2002).
- [117] R. Faller, *Rev. Comp. Ch.* **23**, 233 (2007).
- [118] C. Peter and K. Kremer, *Faraday Discuss.* **144**, 9 (2010).
- [119] O. Hahn, L. D. Site, and K. Kremer, *Macromol. Theory Simul.* **10**, 288 (2001).
- [120] K. Z. Takahashi, R. Nishimura, N. Yamato, K. Yasuoka, and Y. Masubuchi, *Nature* **7**, 12379 (2017).
- [121] G. Ianniruberto, A. Brasiello, and G. Marrucci, *Macromolecules* **45**, 8058 (2012).
- [122] T. Yaoita, T. Isaki, Y. Masubuchi, H. Watanabe, G. Ianniruberto, and G. Marrucci, *Macromolecules* **45**, 2773 (2012).
- [123] S. L. Wingstrand, N. J. Alvarez, Q. Huang, and O. Hassager, *Phys. Rev. Lett.* **115**, 078302 (2015).
- [124] G. Ciccotti, M. Ferrario, and J.-P. Ryckaert, *Mol. Phys.* **47**, 1253 (1982).
- [125] C. C. Hua and J. D. Schieber, *J. Chem. Phys.* **109**, 10018 (1998).
- [126] Y. Masubuchi, J.-I. Takimoto, K. Koyama, G. Ianniruberto, G. Marrucci, and F. Greco, *J. Chem. Phys.* **115**, 4387 (2001).
- [127] A. E. Likhtman, *Macromolecules* **38**, 6128 (2005).
- [128] V. C. Chappa, D. C. Morse, A. Zippelius, and M. Müller, *Phys. Rev. Lett.* **109**, 148302 (2012).
- [129] G. G. Vogiatzis, G. Megariotis, and D. N. Theodorou, *Macromolecules* **50**, 3004 (2017).
- [130] S. J. Marrink, H. J. Risselada, S. Yefimov, D. P. Tieleman, and A. H. De Vries, *J. Phys. Chem. B.* **111**, 7812 (2007).
- [131] A. P. Lyubartsev and A. Laaksonen, *Phys. Rev. E* **52**, 3730 (1995).
- [132] S. Izvekov and G. A. Voth, *J. Chem. Phys.* **123**, 134105 (2005).
- [133] V. Röhle, C. Junghans, A. Lukyanov, K. Kremer, and D. Andrienko, *J. Chem. Theory Comput.* **5**, 3211 (2009).
- [134] H. Mori, *Prog. Theor. Phys.* **33**, 423 (1965).
- [135] S. Nordholm and R. Zwanzig, *J. Stat. Phys.* **13**, 347 (1975).
- [136] C. Hijón, P. Español, E. Vanden-Eijnden, and R. Delgado-Buscalioni, *Faraday Discuss.* **144**, 301 (2010).
- [137] A. Carof, R. Vuilleumier, and B. Rotenberg, *J. Chem. Phys.* **140**, 124103 (2014).
- [138] G. Jung, M. Hanke, and F. Schmid, *J. Chem. Theory Comput.* **13**, 2481 (2017).
- [139] T. Soddemann, B. Dünweg, and K. Kremer, *Phys. Rev. E* **68**, 046702 (2003).
- [140] L. A. Moreira, G. Zhang, F. Müller, T. Stuehn, and K. Kremer, *Macromol. Theory Simul.* **24**, 419 (2015).
- [141] C. Svaneborg, H. A. Karimi-Varzaneh, N. Hojdis, F. Fleck, and R. Everaers, *Phys. Rev. E* **94**, 032502 (2016).
- [142] T. W. Sirk, Y. R. Slizoberg, J. K. Brennan, M. Lisal, and J. W. Andzelm, *J. Chem. Phys.* **136**, 134903 (2012).
- [143] I. Carmesin and K. Kremer, *Macromolecules* **21**, 2819 (1988).
- [144] V. Tries, W. Paul, J. Baschnagel, and K. Binder, *J. Chem. Phys.* **106**, 738 (1997).
- [145] M. Baiesi, G. T. Barkema, and E. Carlon, *Phys. Rev. E* **81**, 061801 (2010).
- [146] R. Schram and G. Barkema, *J. Comput. Phys.* **363**, 128 (2018).
- [147] R. Everaers, S. K. Sukumaran, G. S. Grest, C. Svaneborg, A. Sivasubramanian, and K. Kremer, *Science* **303**, 823 (2004).
- [148] P. Carbone, H. A. Karimi-Varzaneh, and F. Müller-Plathe, *Faraday Discuss.* **144**, 25 (2010).
- [149] W. Zhang, E. D. Gomez, and S. T. Milner, *Phys. Rev.*

- Lett. **119**, 017801 (2017).
- [150] C. Bennemann, J. Baschnagel, W. Paul, and K. Binder, *Comput. Theor. Polym. Sci.* **9**, 217 (1999).
- [151] J. Baschnagel and F. Varnik, *J. Phys.: Condens. Matter* **17**, R851 (2005).
- [152] M. L. Williams, R. F. Landel, and J. D. Ferry, *J. Am. Chem. Soc.* **77**, 3701 (1955).

Table of content graphic

Kremer-Grest models for commodity polymer melts: Linking theory, experiment and simulation at the Kuhn scale.

Carsten Svaneborg, Hossein Ali Karimi-Varzaneh, Nils Hojdis, Frank Fleck, and Ralf Everaers.

